Electronic Supplementary Information (ESI)

The multifunctional design of metal-organic framework by applying linker desymmetrization strategy: synergistic catalysis for high CO_2-epoxides conversion

Yueying Zhu, Jiaming Gu, Xueyue Yu, Borong Zhang, Guanghua Li, Jiantang Li,* and Yunling Liu*

State Key Laboratory of Inorganic Synthesis and Preparative Chemistry, College of Chemistry, Jilin University, Changchun 130012, P. R. China. Fax: +86-431-85168624; Tel: +86-431-85168614; E-mail: yunling@jlu.edu.cn, lijt1992@163.com.

Table of Contents

S1. Calculation procedures of selectivity from IAST

The measured experimental data is excess loadings (q^{ex}) of the pure components CO_2, CH_4, C_2H_2, C_2H_4 C_2H_6 and C_3H_8 for compound **1**, which should be converted to absolute loadings (q) firstly.

$$q = q^{ex} + \frac{pV_{pore}}{ZRT} \quad (1)$$

Here Z is the compressibility factor. The Peng-Robinson equation (Eq. 1) is used to estimate the value of compressibility factor to obtain the absolute loading, while the measure pore volume is also necessary. The dual-site Langmuir-Freundlich equation (Eq. 2) is used for fitting the isotherm data at 298 K.

$$q = q_{m_1} \times \frac{b_1 \times p^{1/n_1}}{1 + b_1 \times p^{1/n_1}} + q_{m_2} \times \frac{b_2 \times p^{1/n_2}}{1 + b_2 \times p^{1/n_2}} \quad (2)$$

Here p is the pressure of the bulk gas at equilibrium with the adsorbed phase (kPa), q is the adsorbed amount per mass of adsorbent (mol kg^{-1}), q_{m1} and q_{m2} are the saturation capacities of sites 1 and 2 (mol kg^{-1}), b_1 and b_2 are the affinity coefficients of sites 1 and 2 (1/kPa), n_1 and n_2 are the deviations from an ideal homogeneous surface.

$$S = \frac{q_1/q_2}{p_1/p_2} \quad (3)$$

The selectivity of preferential adsorption of component 1 over component 2 in a mixture containing 1 and 2, perhaps in the presence of other components too, can be formally defined as q_1 and q_2 are the absolute component loadings of the adsorbed phase in the mixture. These component loadings are also termed the uptake capacities. We calculate the values of q_1 and q_2 using the Ideal Adsorbed Solution Theory (IAST) of Myers and Prausnitz (Eq. 3).

S2. Details of experiments and calculation procedures of catalytic efficiency

In the high-pressure catalytic reaction, epoxide (20 mmol), TBAB (1 mmol, 5 mol %), activated compound **1** (0.5 mol % open Cu sites) were put into a high-pressure reactor. To activate the MOFs materials, the as-synthesized samples were activated with the exchange of methanol solvent 8 times in 1 day at 85 °C oven. After that, the samples were dried in the vacuum condition for 10 h at 85 °C and collected the MOFs for further cycloaddition reaction.

Before triggering the reaction, pump out the air inside the reactor and fill in with pure CO_2. After 3 times pump-fill procedure, turn the temperature and pressure to specific conditions (2 MPa, 60 °C, 6 h). The speed of stirring was 400 rpm. After centrifuging to recycle the catalyst, a little supernatant reaction mixture was taken to analyze by ^{1}H NMR.

The yields of PO, 1, 2-epoxy-3-phenoxypropane, glycidyl-2-methylphenyl ether and cyclohexene oxide (H_a for epoxides and $H_{a'}$ for carbonates, respectively) catalyzed by compound **1** were calculated according to the following equation (Eq. 4).

$$Yield(\%) = \frac{I_{Ha'}}{I_{H_a} + I_{Ha'}} \times 100\% \quad (4)$$

The yield of SO to styrene carbonate were determined by calculation of the ^{1}H NMR integrals of corresponding highlighted protons in styrene oxide (H_a), styrene carbonate ($H_{a'}$) and phenyl group (H_b-H_f)

(from SO, styrene carbonate and other by-products) according to the following equation (Eq. 5).

$$Yield(\%) = \frac{5 \times I_{H_{a'}}}{I_{H_b - H_f}} \times 100\% \quad (5)$$

S3. Supporting Figures

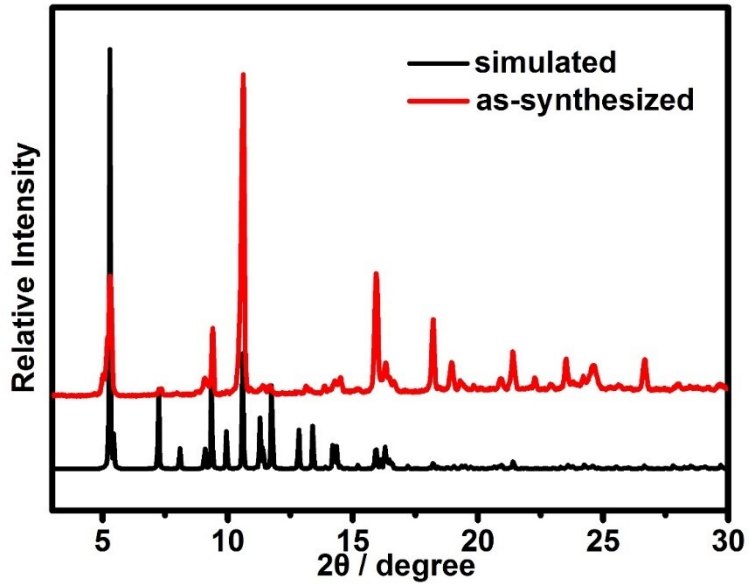

Fig. S1 Simulated and as-synthesized PXRD patterns of compound **1**.

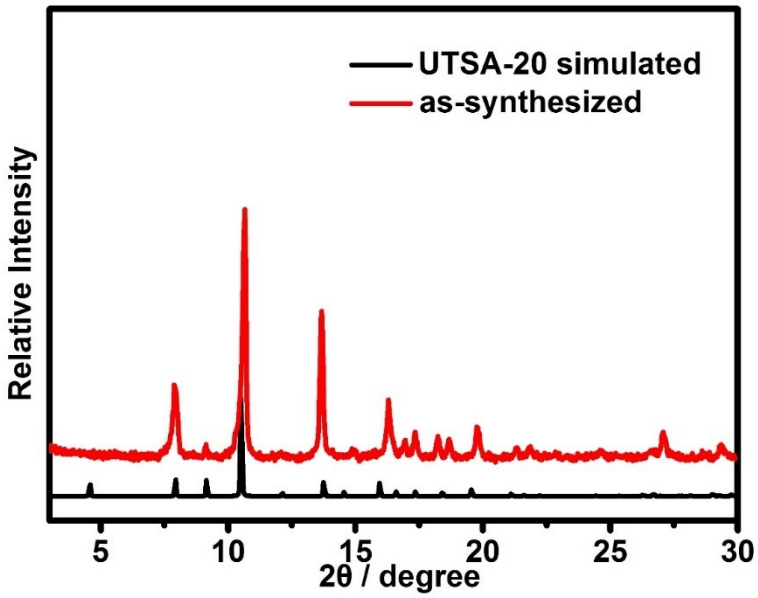

Fig. S2 Simulated and as-synthesized PXRD patterns of UTSA-20.[1]

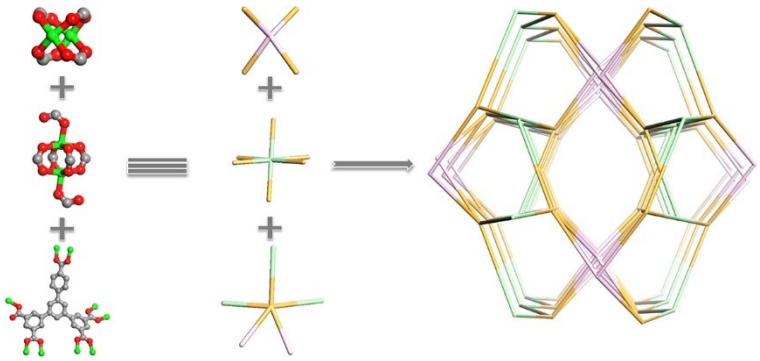

Fig. S3 Topology simplification of organic and inorganic SBUs as well as (4, 5, 6)-connected topology.

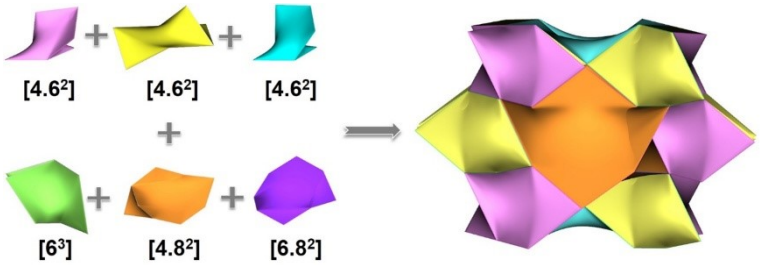

Fig. S4 Topological features of compound **1** displayed by tiles and face symbols.

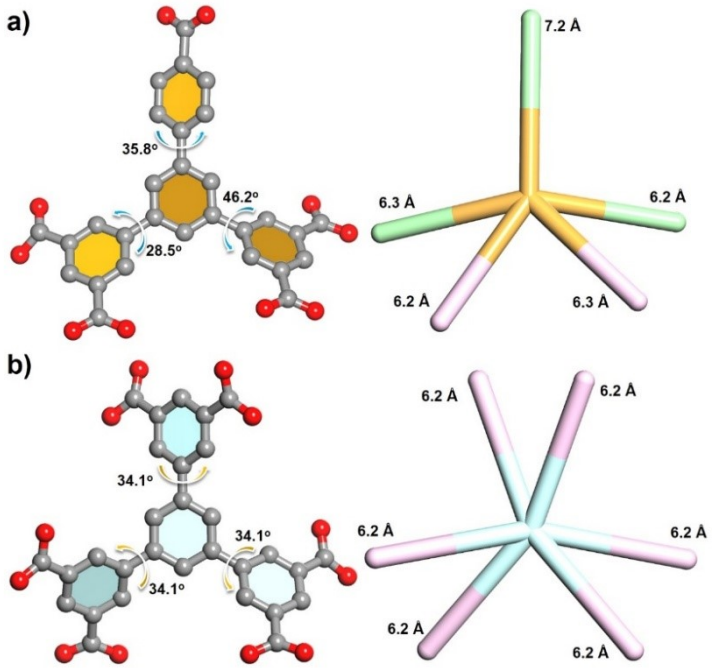

Fig. S5 a) Different torsion angles and diverse distances of $CPTPTA^{5-}$ ligand in compound **1**; b) torsion angles and distances of BHB ligand in UTSA-20.

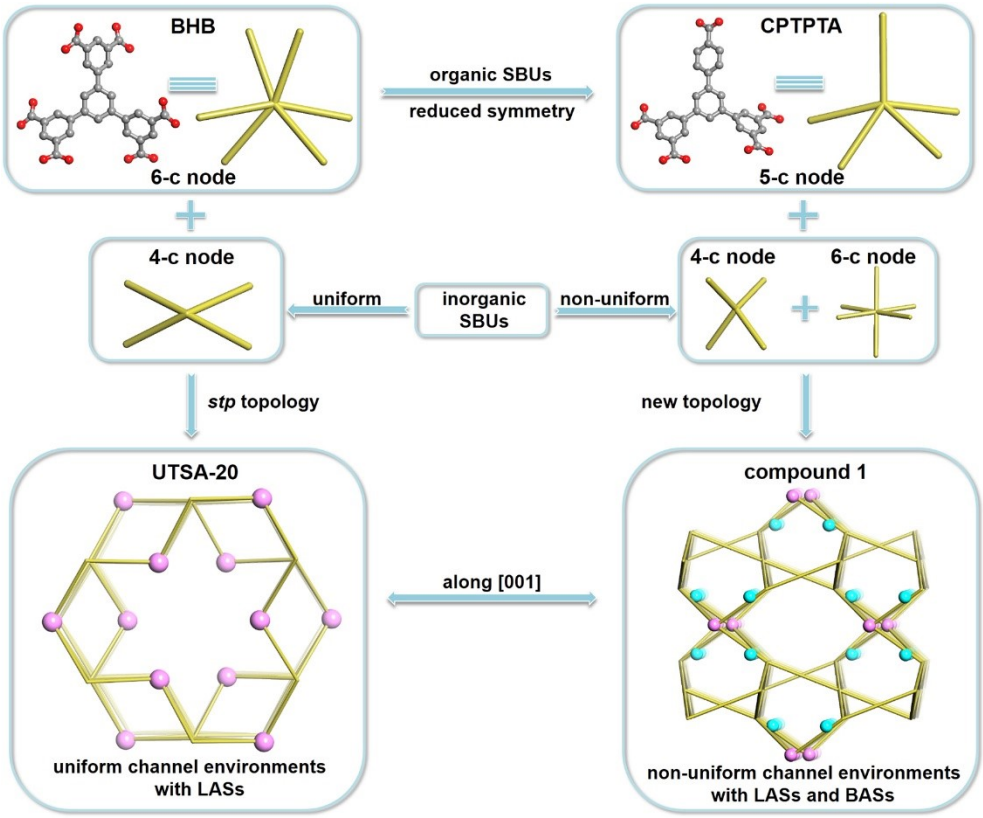

Fig. S6 Structure, topology, and catalysis site comparisons between UTSA-20 (left) and compound **1** (right).

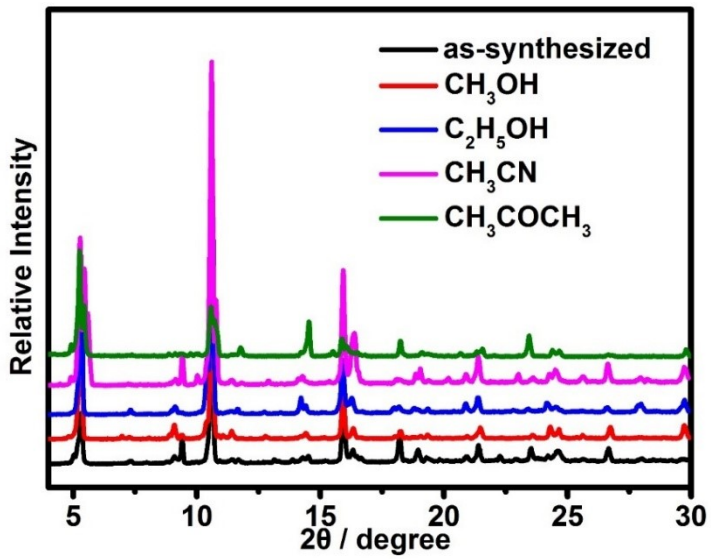

Fig. S7 PXRD patterns of compound **1** soaking in different common organic solvents.

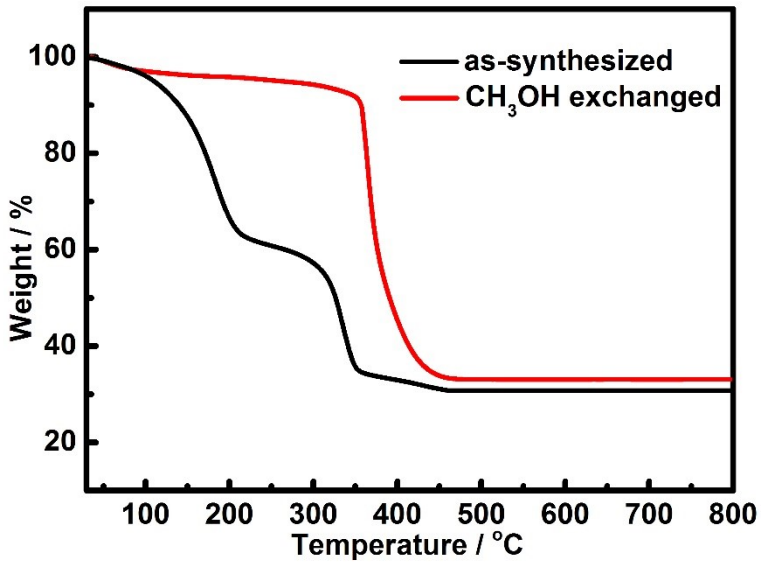

Fig. S8 Thermogravimetric analysis curves of compound **1** for the as-synthesized samples and CH_3OH exchanged samples.

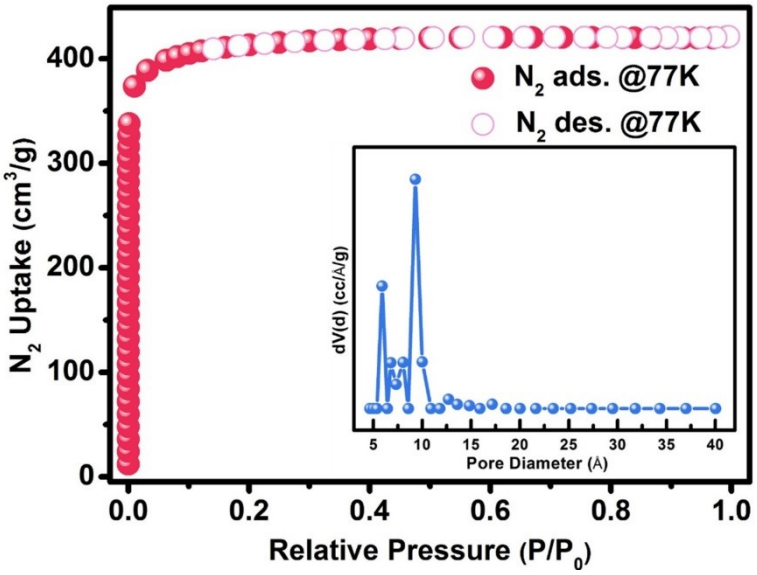

Fig. S9 N_2 adsorption isotherm of compound **1** under 77 K; (inset) pore size distribution of compound **1**.

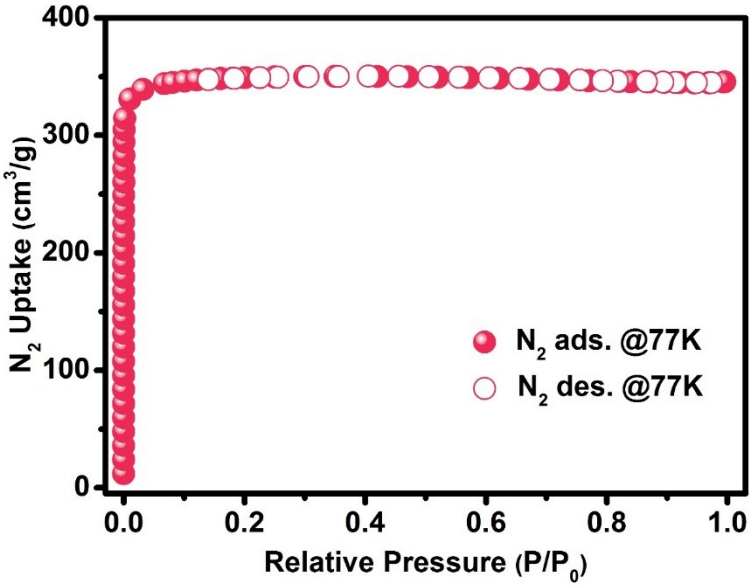

Fig. S10 N_2 adsorption isotherm of UTSA-20 under 77 K.

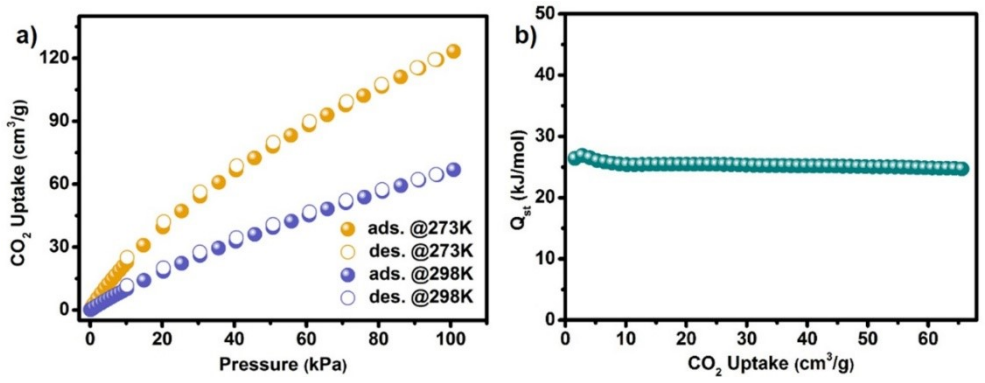

Fig. S11 (a) CO_2 adsorption isotherms of compound **1** at 273 K and 298 K; (b) Q_{st} of CO_2 for compound **1**.

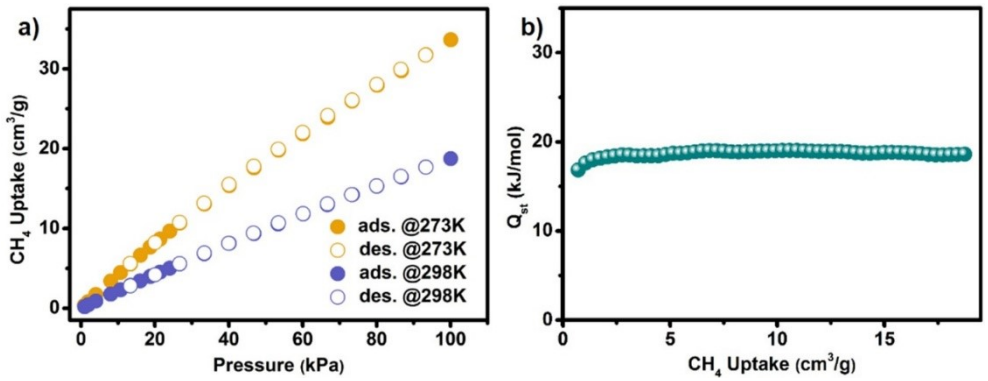

Fig. S12 (a) CH_4 adsorption isotherms of compound **1** at 273 K and 298 K; (b) Q_{st} of CH_4 for compound **1**.

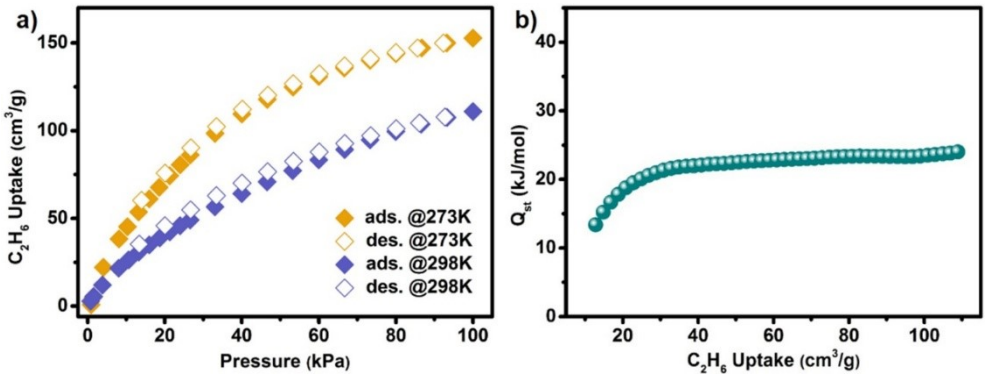

Fig. S13 (a) C_2H_6 adsorption isotherms of compound **1** at 273 K and 298 K; (b) Q_{st} of C_2H_6 for compound **1**.

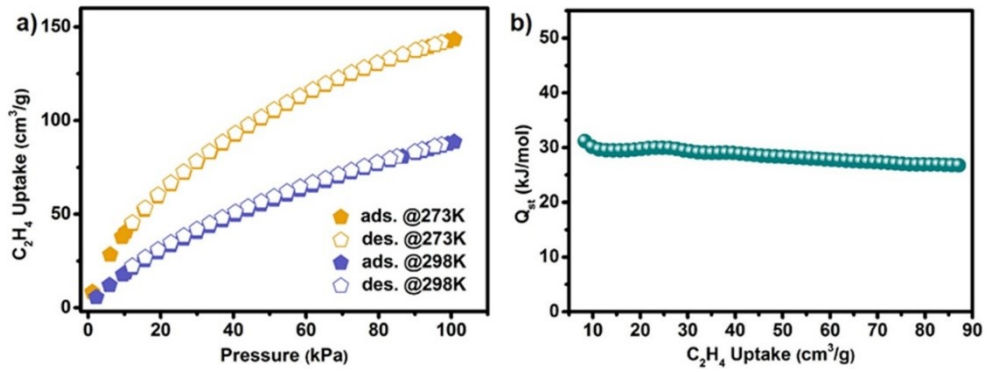

Fig. S14 (a) C_2H_4 adsorption isotherms of compound **1** at 273 K and 298 K; (b) Q_{st} of C_2H_4 for compound **1**.

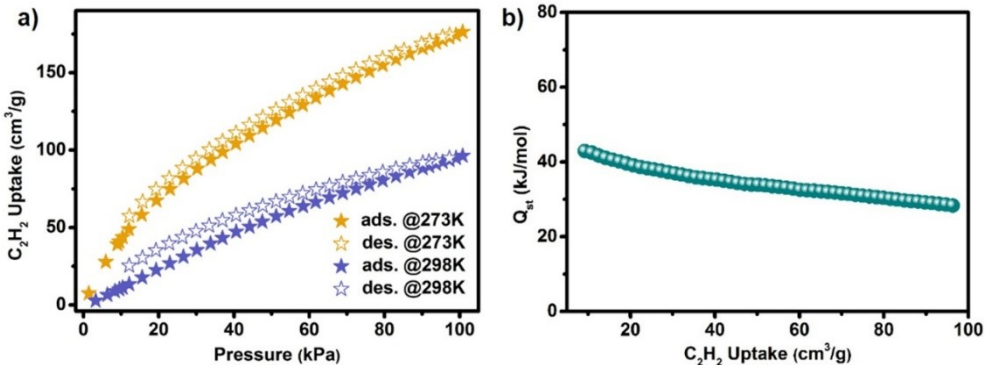

Fig. S15 (a) C_2H_2 adsorption isotherms of compound **1** at 273 K and 298 K; (b) Q_{st} of C_2H_2 for compound **1**.

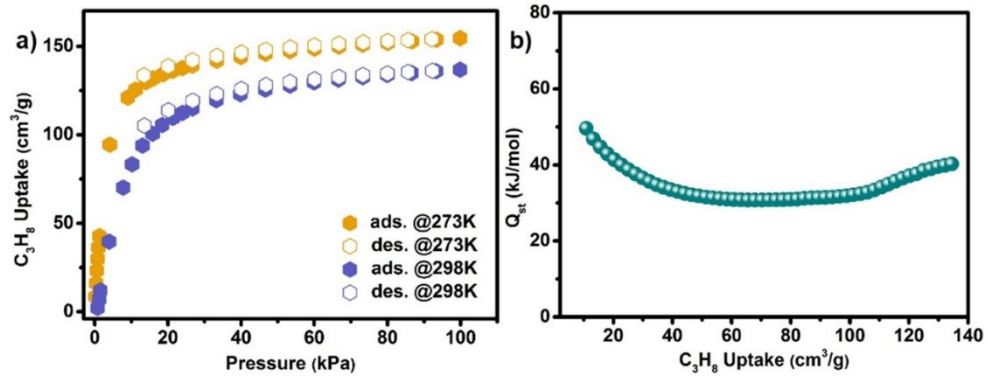

Fig. S16 (a) C_3H_8 adsorption isotherms of compound **1** at 273 K and 298 K; (b) Q_{st} of C_3H_8 for compound **1**.

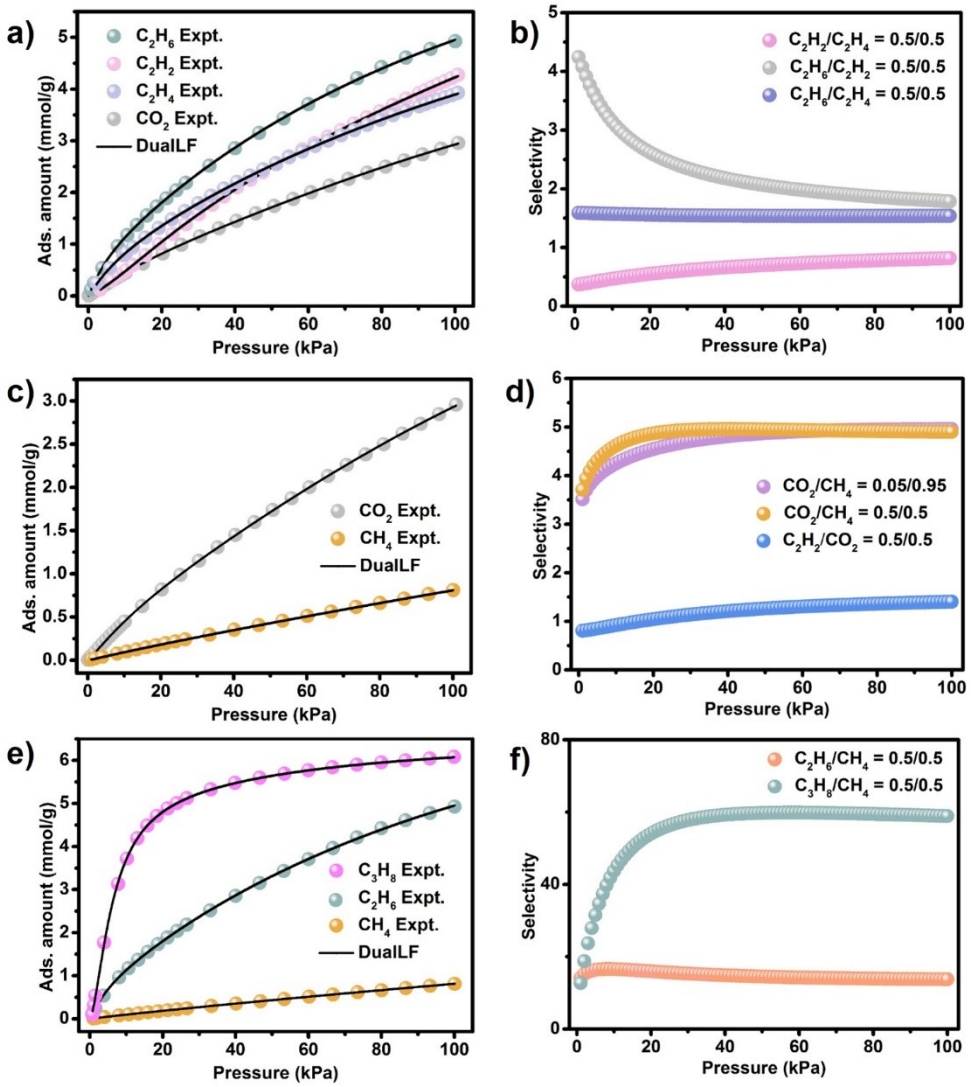

Fig. S17 Gas adsorption isotherms at 298 K along with the dual-site Langmuir Freundlich (DSLF) fits (a, c and e) and adsorption selectivity predicted by the Ideal Adsorbed Solution Theory (IAST) at 298 K, 1 atm for compound **1** (b, d and f).

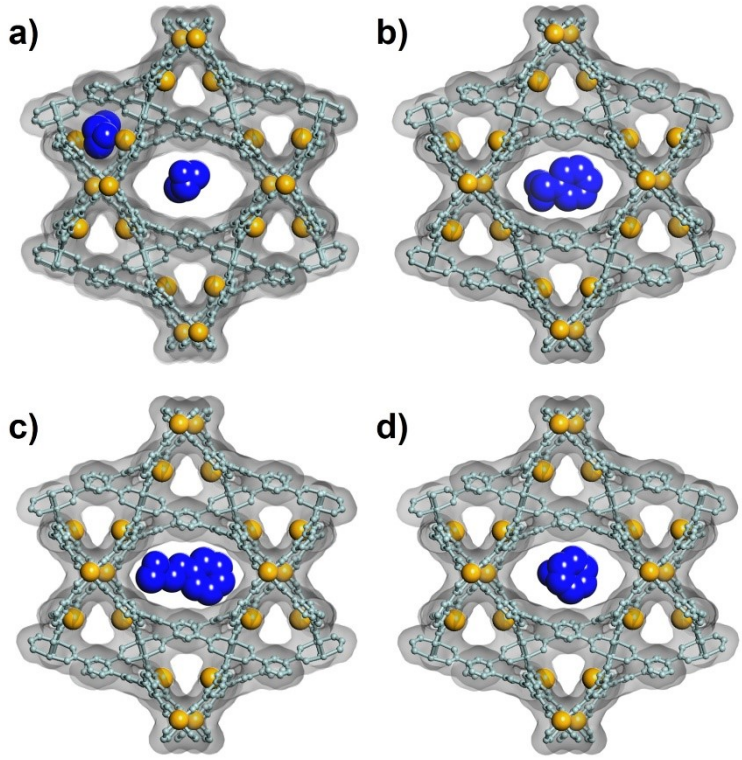

Fig. S18 Simulated CPK models of epoxides in channels for compound **1** (color scheme: active sites = yellow, structure of compound **1** = light blue, epoxides = dark blue).

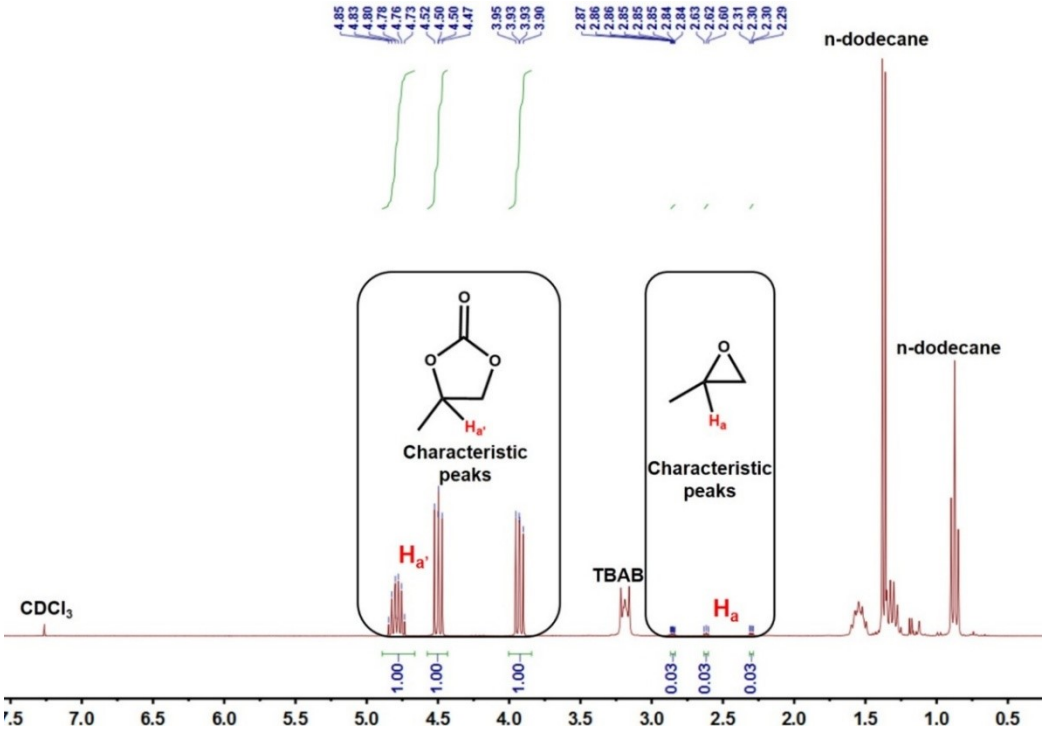

Fig. S19 ^{1}H NMR spectrum of the mixture produced by cycloaddition reaction of propylene oxide catalyzed by compound **1** in $CDCl_3$. n-dodecane was used as internal standard.

Sixteen parallel experiments for 20 min, 40 min, 1 h, 2 h, 3 h, 4 h, 5 h and 6 h of run 1 and run 5 with the optimized conditions (0.5 mol % Cu sites along with 0.5 mol % protonated carboxylic acid sites and 5 mol % TBAB under 60 °C at 2 MPa for 6 h) were executed to investigate the influence of reaction time on PC's yield. As shown in Fig. S20 (ESI†), before 40 min the curves raised rapidly, which showed that the reaction was within the kinetic interval. From 40 min to 6 h, the decline of the curve slope displayed that the inflexion existed in the interval. In run 5, the yield reduced, which may cause by the declension of compound **1**'s crystallization.

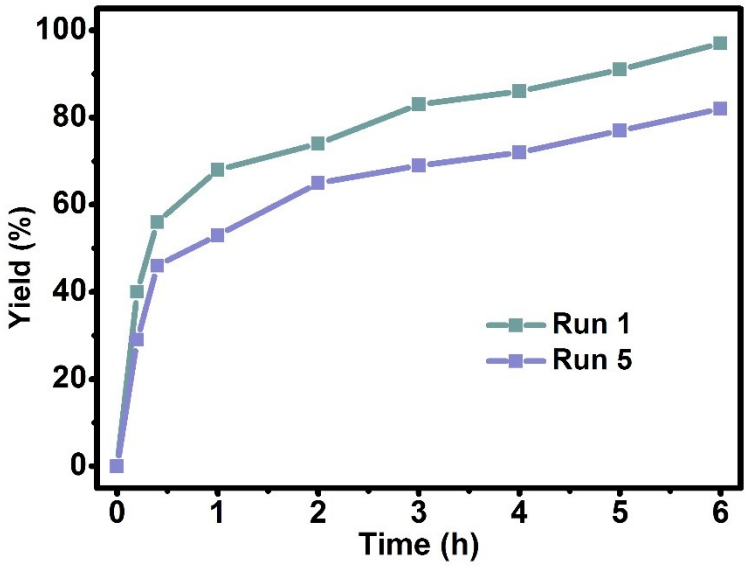

Fig. S20 Kinetic curves of CO_2-PO cycloaddition catalyzed by compound **1** (color scheme: green = run 1; purple = run 5).

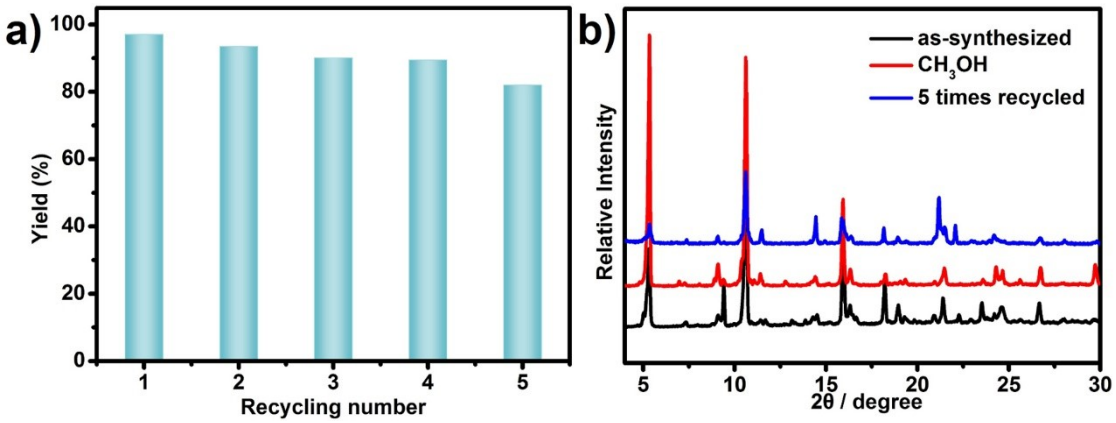

Fig. S21 (a) Recycling experiments of the cycloaddition reaction of PO with CO_2 with compound **1**; (b) PXRD patterns of compound **1** after 5 times recycled.

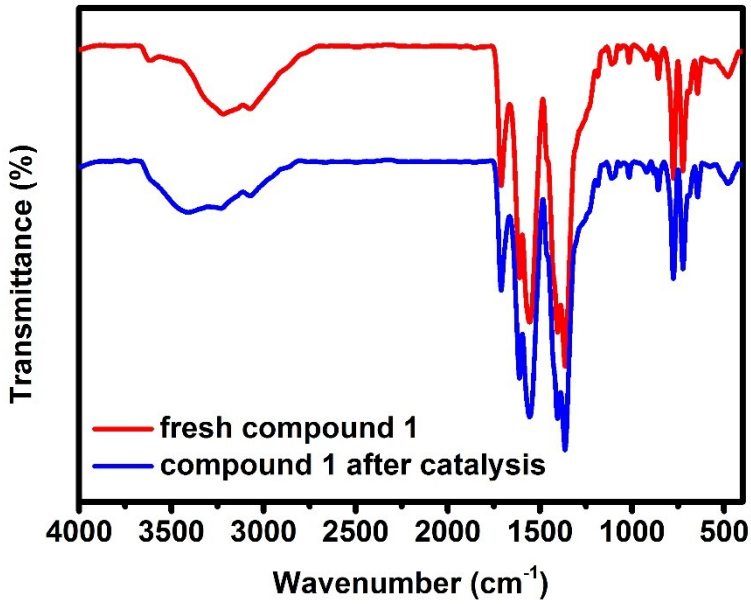

Fig. S22 FT-IR spectra of fresh compound **1** and compound **1** after catalysis.

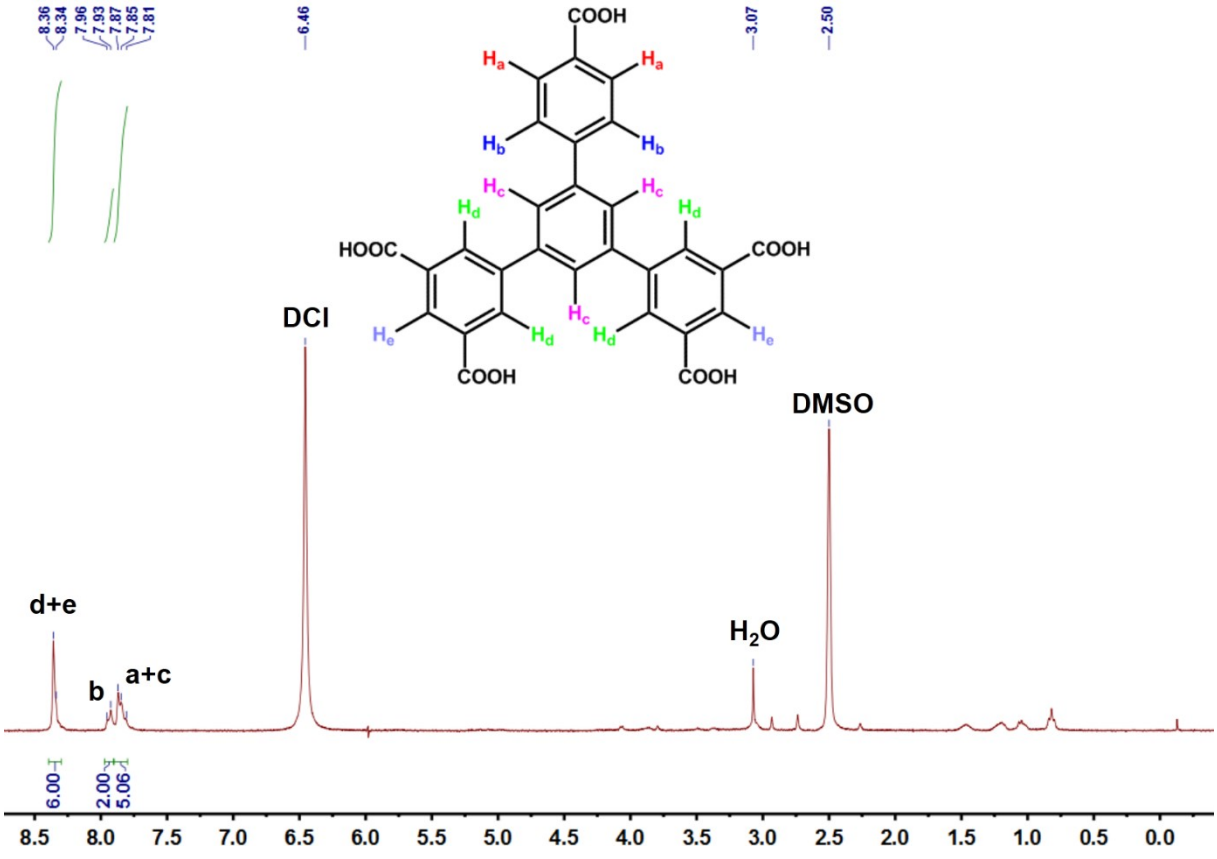

Fig. S23 ^{1}H NMR spectrum of compound **1** after 5 times recycle in DCl and DMSO.

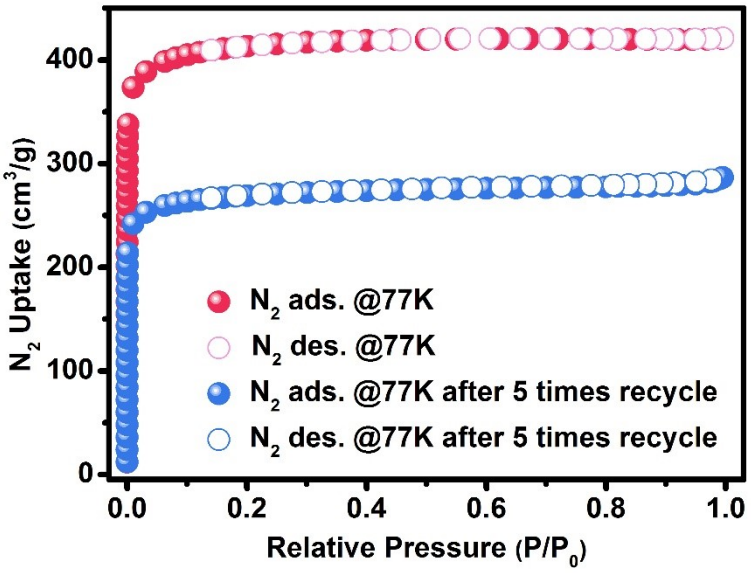

Fig. S24 N_2 adsorption isotherm at 77 K of activated compound **1** (red) and compound **1** after 5 times recycle (blue).

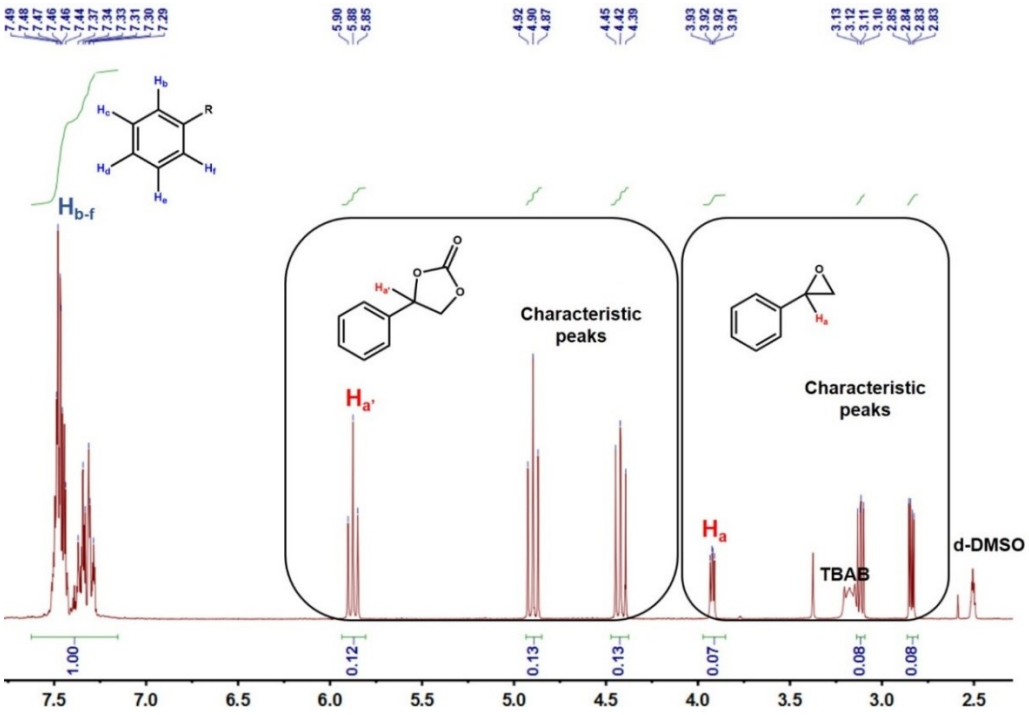

Fig. S25 ^{1}H NMR spectrum of the mixture produced by cycloaddition reaction of styrene oxide catalyzed by compound **1** in d-DMSO.

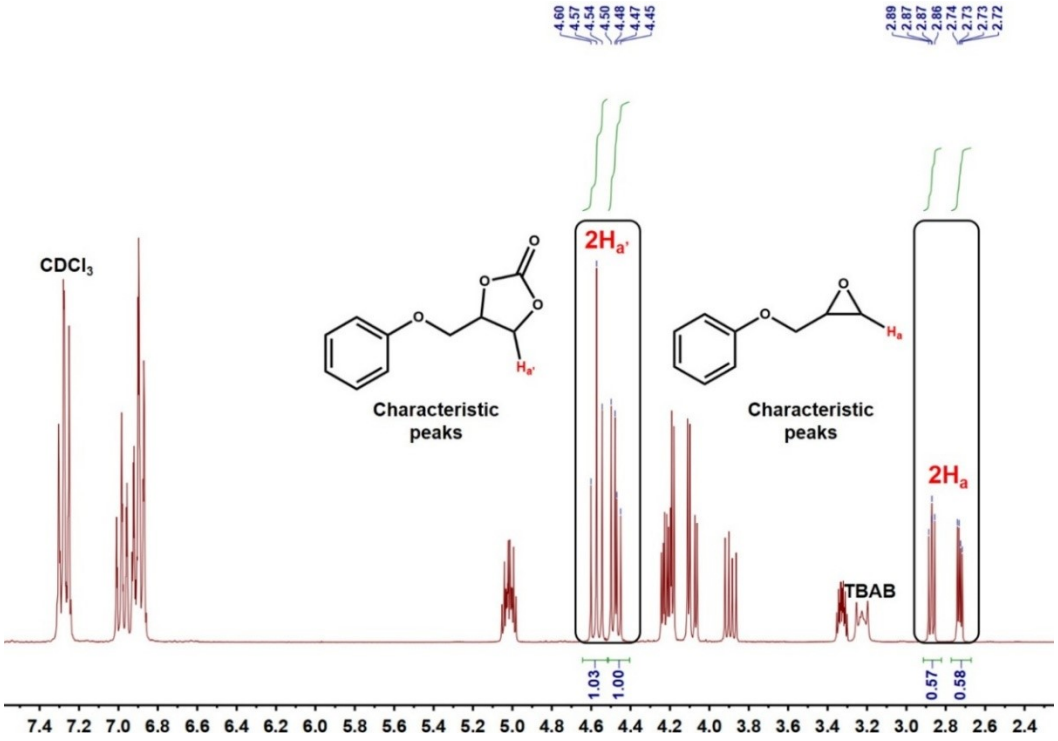

Fig. S26 ^{1}H NMR spectrum of the mixture produced by cycloaddition reaction of 1, 2-epoxy-3-phenoxypropane catalyzed by compound **1** in $CDCl_3$.

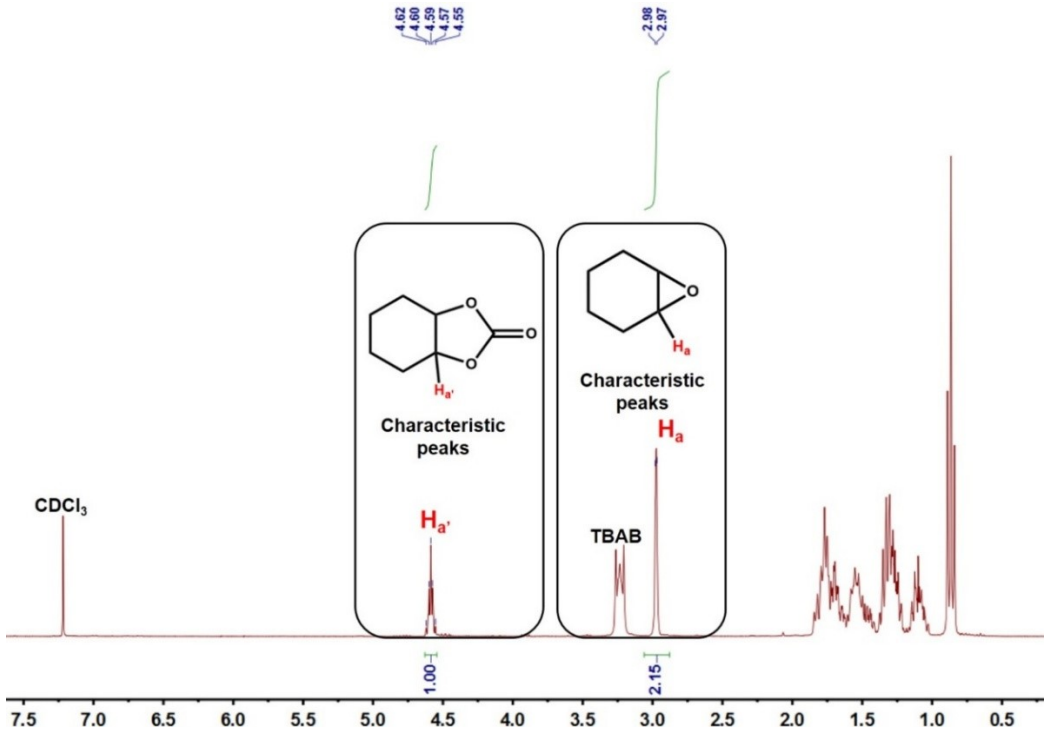

Fig. S27 ^{1}H NMR spectrum of the mixture produced by cycloaddition reaction of cyclohexene oxide catalyzed by compound **1** in $CDCl_3$.

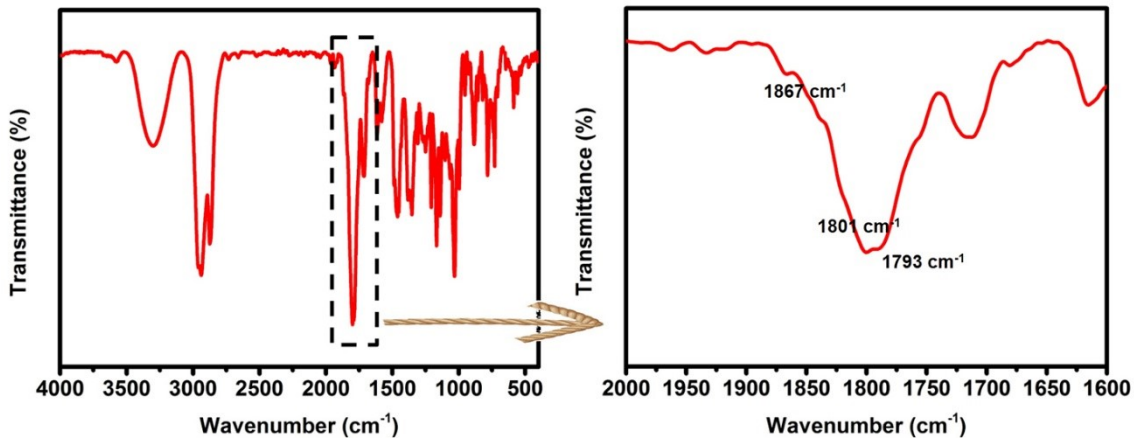

Fig. S28 FT-IR spectra of *cis*- cyclic cyclohexyl carbonate.

S4. Supporting Tables

Table S1. Crystal data and structure refinements for compound **1**.

compound	**Compound 1**
Formula	$C_{44}\ H_{64}\ Cu_2\ N_8\ O_{22}$
Formula weight	1184.11
Temperature (K)	293(2)
Wavelength (Å)	0.71073
Crystal system	Monoclinic
Space group	*C*2/*c*
a (Å)	33.183(7)
b (Å)	19.468(4)
c (Å)	16.287(3)
α (°)	90
β (°)	102.34(3)
γ (°)	90
V (Å^3)	10279(4)
Z, D_c (Mg/m^3)	8, 1.530
F(000)	4944
ϑ range (deg)	2.292-25.379
reflns collected/unique	40505/9423
R_{int}	0.0321
data/restraints/params	9423/15/388
GOF on F^2	1.086
R_1, wR_2 (I>2σ(I))	0.0353, 0.1100
R_1, wR_2 (all data)	0.0407, 0.1124

[a]$R_1 = \Sigma||F_o| - |F_c||/\Sigma|F_o|$, [b]$wR_2 = [\Sigma w(|F_o|^2 - |F_c|^2)/\Sigma|w(F_o^2)^2|]^{1/2}$

Table S2. Selected bond lengths [Å] and angles [º] for compound **1**.

Compound 1			
Cu(1)-O(6)#1	1.9634(19)	O(7)#5-Cu(2)-O(3)	173.33(8)
Cu(1)-O(2)#2	1.9655(19)	O(7)#5-Cu(2)-O(8)#6	88.14(9)
Cu(1)-O(1)	1.977(2)	O(3)-Cu(2)-O(8)#6	88.06(9)
Cu(1)-O(5)#3	1.981(2)	O(7)#5-Cu(2)-O(4)#7	89.65(8)
Cu(1)-O(9)#4	2.1256(19)	O(3)-Cu(2)-O(4)#7	92.29(8)
Cu(1)-Cu(1)#2	2.7161(8)	O(8)#6-Cu(2)-O(4)#7	162.01(7)
Cu(2)-O(7)#5	1.9254(18)	O(7)#5-Cu(2)-O(11)	93.92(10)
Cu(2)-O(3)	1.9348(17)	O(3)-Cu(2)-O(11)	92.23(10)
Cu(2)-O(8)#6	2.0134(18)	O(8)#6-Cu(2)-O(11)	102.24(10)
Cu(2)-O(4)#7	2.0155(17)	O(4)#7-Cu(2)-O(11)	95.72(9)
Cu(2)-O(11)	2.137(2)	O(7)#5-Cu(2)-Cu(2)#7	86.12(6)
Cu(2)-Cu(2)#7	2.6227(8)	O(3)-Cu(2)-Cu(2)#7	87.91(6)
O(6)#1-Cu(1)-O(2)#2	90.23(9)	O(8)#6-Cu(2)-Cu(2)#7	81.68(6)
O(6)#1-Cu(1)-O(1)	88.42(10)	O(4)#7-Cu(2)-Cu(2)#7	80.35(6)
O(2)#2-Cu(1)-O(1)	165.72(8)	O(11)-Cu(2)-Cu(2)#7	176.08(8)
O(6)#1-Cu(1)-O(5)#3	165.94(8)	C(13)-O(1)-Cu(1)	126.83(18)
O(2)#2-Cu(1)-O(5)#3	87.28(9)	C(13)-O(2)-Cu(1)#2	122.13(18)
O(1)-Cu(1)-O(5)#3	90.59(10)	C(20)-O(3)-Cu(2)	119.08(16)
O(6)#1-Cu(1)-O(9)#4	103.26(8)	C(20)-O(4)-Cu(2)#7	124.85(16)
O(2)#2-Cu(1)-O(9)#4	102.19(9)	C(21)-O(5)-Cu(1)#8	123.77(17)
O(1)-Cu(1)-O(9)#4	91.95(9)	C(21)-O(6)-Cu(1)#4	124.39(16)
O(5)#3-Cu(1)-O(9)#4	90.80(8)	C(28)-O(7)-Cu(2)#5	121.91(17)
O(6)#1-Cu(1)-Cu(1)#2	83.11(6)	C(28)-O(8)-Cu(2)#9	122.69(16)
O(2)#2-Cu(1)-Cu(1)#2	85.15(6)	C(29)-O(9)-Cu(1)#1	125.4(2)
O(1)-Cu(1)-Cu(1)#2	80.58(6)	Cu(2)-O(11)-H(11A)	115(2)
O(5)#3-Cu(1)-Cu(1)#2	82.89(6)	Cu(2)-O(11)-H(11B)	111(2)
O(9)#4-Cu(1)-Cu(1)#2	170.13(6)		

Symmetry transformations used to generate equivalent atoms:

#1 -x+1/2, -y+1, z-1/2 #2 x-1/2, y, -z+3/2 #3 x, -y+3/2, z #4 x+1/2, y, -z+1/2

#5 x+1/2, -y+3/2, -z+1/2 #6 x+1/2, y, -z+3/2 #7 -x+1/2, -y+1, z+1/2 #8 x-1/2, y, -z+1/2

Table S3. Comparisons about CO_2 uptakes under 1 atm at 273 K and 298 K of some selected MOFs.

Compounds	BET ($m^2 g^{-1}$)	273 K CO_2 uptake (mmol g^{-1})	298 K CO_2 uptake (mmol g^{-1})	Ref.
Mg_2(dobpdc)	3270	N.A.	6.4	2
UTSA-20	1156	N.A.	5.2 (300 K)	1
MAF-66	1014	6.3	4.4	3
HKUST-1	1507	N.A.	4.1	4
Compound 1	1355	5.5	3.0	This work
IFMC	780	4.1	2.7	5
MAF-23	622 (Langmuir)	3.3	2.5	6
NH_2-MIL-125	1469	4.0	2.2	7
USTC-253	1800	3.7	2.1	8
SNU-M10	505 (Langmuir)	3.3	2.1	9
1	385	2.8	1.6	10
Py-UiO-66	537	N.A.	1.4	11
TMOF-1	256	2.2	1.4	12
SNU-5	2189 (Langmuir)	0.9	N.A.	13

Table S4. Comparisons about cycloaddition reaction of CO_2 with PO of some selected MOFs.

Entry	Catalysts	Tem. /°C	P /MPa	Time /h	Yield /%	Ref.
1	MIL-101-N(*n*-Bu)$_3$Br [a]	80	2	8	99.1	14
2	$Zn_3(L)_3(H_2L)$ [b]	80	1	5	99	15
	$Zn_3(L)_3(H_2L)$ [c]	30		24	99	
3	Gd-MOF [d]	80	2	5	98.4	16
4	MOF-5 [e]	50	6	4	97.6	17
5	**Compound 1**	60	2	6	97	This work
6	RD Au/Zn-MOF nanocages [f]	70	3	6	96	18
7	NOTT-100	55	0.2	48	66	19
	NOTT-100-Py1				81	
	NOTT-100-Py2				96	
	NOTT-100-Py3				91	
	NOTT-100-H3 [g]				90	
8	*int*-MOF-5 [h]	50	5.5	0.5	94	20
9	MIL-101-NHIM-NH_2 [i]	120	2	4	93.5	21
10	JLU-Liu22 [j]	60	2	6	92	22
11	Zn(L)(aip)(H_2O) [k]	100	3	6	92	23
12	**gea**-MOF-1 [l]	120	2	6	88	24
13	Ni(salphen)-MOF [m]	80	2	4	80	25

Reaction conditions: [a] PO (30 mmol), catalyst (0.27 mmol). [b] PO (34.5 mmol), catalyst (0.1 g, $Zn_3(L)_3(H_2L)$ mol % = 0.27, Zn mol % = 0.05, Bu_4NBr mol % = 3.6). [c] PO (34.5 mmol), catalyst (0.1 g), TBAB (0.4 g). [d] PO (20 mmol), catalyst (100 mg), TBAB (2.5 mol %). [e] PO (20 mmol), catalyst (100 mg), TBAB (2.5 mol %). [f] PO (10 mmol), catalyst (32 mg). [g] PO (10 mmol), catalyst (0.5 mol %, calculated based on Cu content), TBAB (2 mmol, 10 mol %). [h] PO (25 mmol), catalyst (0.0325 mmol), TBAB (0.242 mmol). [i] PO (34.5 mmol), catalyst (0.2 g). [j] PO (40 mmol), catalyst (0.25 mol % open Cu sites), TBAB (2 mmol). [k] PO (3.5 mL), catalyst (0.07 mmol). [l] PO (100 mmol), catalyst (60 mg, 0.15 mmol Y^{3+}), TBAB (0.15 mmol). [m] PO (10 mmol), catalyst (0.05 g), TBAB (3 mol %).

Table S5. Crystal data comparisons of compound **1** and UTSA-20.

	Compound 1	**UTSA-20**
Crystal system	Monoclinic	Hexagonal
Space group	*C*2/*c*	$P6_3/mcm$
a (Å)	33.183	22.287
b (Å)	19.468	22.287
c (Å)	16.287	12.816
α (°)	90	90
β (°)	102.34	90
γ (°)	90	120
V (Å^3)	10279	5513
BET surface area ($m^2\ g^{-1}$)	1355	1156
Pore volume ($cm^3\ g^{-1}$)	0.65	0.63

Table S6. Comparisons about cycloaddition reaction of CO_2 with 20 mmol PO catalyzed by compound **1** and UTSA-20.

Entry	**Compounds**	**TBAB**	**Tem. /°C**	**P /MPa**	**Time /h**	**Yield /%**
1	Compound 1 (0.5 mol % LASs and 0.5 mol % BASs)	5 mol %	60	2	6	97
2	UTSA-20 (0.5 mol % LASs)	5 mol %	60	2	6	65
3	UTSA-20 (1 mol % LASs)	5 mol %	60	2	6	74

Table S7. ICP-OES analysis of Cu^{2+} after the 5th time reaction.

Catalyst	**Cu^{2+} concentration (ppm)**
Compound 1	0.0187

Table S8. Sizes of epoxides selected for the experiments.[22]

Epoxides	**Volume**
Propylene oxide	6.1 Å × 4.4 Å × 5.0 Å
Styrene oxide	9.3 Å × 6.9 Å × 4.6 Å
1,2-epoxy-3-phenoxypropane	12.5 Å × 7.1 Å × 5.4 Å
Cyclohexene oxide	6.5 Å × 7.0 Å × 5.0 Å

References

1 Z. Guo, H. Wu, G. Srinivas, Y. Zhou, S. Xiang, Z. Chen, Y. Yang, W. Zhou, M. O'Keeffe, B. Chen, A metal–organic framework with optimized open metal sites and pore spaces for high methane storage at room temperature, *Angew. Chem. Int. Ed.*, 2011, **50**, 3178-3181.

2 T. M. McDonald, W. R. Lee, J. A. Mason, B. M. Wiers, C. S. Hong, J. R. Long, Capture of carbon dioxide from air and flue gas in the alkylamine-appended metal-organic framework mmen-Mg_2(dobpdc), *J. Am. Chem. Soc.*, 2012, **134**, 7056-7065.

3 R.-B. Lin, D. Chen, Y.-Y. Lin, J.-P. Zhang, X.-M. Chen, A zeolite-like zinc triazolate framework with high gas adsorption and separation performance, *Inorg. Chem.*, 2012, **51**, 9950-9955.

4 A. R. Millward, O. M. Yaghi, Metal-organic frameworks with exceptionally high capacity for storage of carbon dioxide at room temperature, *J. Am. Chem. Soc.*, 2005, **127**, 17998-17999.

5 J.-S. Qin, D.-Y. Du, W.-L. Li, J.-P. Zhang, S.-L. Li, Z.-M. Su, X.-L. Wang, Q. Xu, K.-Z. Shao, Y.-Q. Lan, N-rich zeolite-like metal–organic framework with sodalite topology: high CO_2 uptake, selective gas adsorption and efficient drug delivery, *Chem. Sci*., 2012, **3**, 2114-2118.

6 P.-Q. Liao, D.-D. Zhou, A.-X. Zhu, L. Jiang, R.-B. Lin, J.-P. Zhang, X.-M. Chen, Strong and dynamic CO_2 sorption in a flexible porous framework possessing guest chelating claws, *J. Am. Chem. Soc.*, 2012, **134**, 17380-17383.

7 S.-N. Kim, J. Kim, H.-Y. Kim, H.-Y. Cho, W.-S. Ahn, Adsorption/catalytic properties of MIL-125 and NH_2-MIL-125, *Catal. Today*, 2013, **204**, 85-93.

8 Z.-R. Jiang, H. Wang, Y. Hu, J. Lu, H.-L. Jiang, Polar group and defect engineering in a metal-organic framework: synergistic promotion of carbon dioxide sorption and conversion, *ChemSusChem*, 2015, **8**, 878-885.

9 H.-S. Choi, M. P. Suh, Highly selective CO_2 capture in flexible 3D coordination polymer networks, *Angew. Chem. Int. Ed.*, 2009, **48**, 6865-6869.

10 G. Chakraborty, P. Das, S. K. Mandal, Efficient and highly selective CO_2 capture, separation, and chemical conversion under ambient conditions by a polar-group-appended copper(II) metal–organic framework, *Inorg. Chem.*, 2021, **60**, 5071-5080.

11 Y.-L. Liu, Y. Di, F. Chen, C. Zhou, B. Liu, A pyridyl-decorated Zr-organic framework for enhanced gas separation and CO_2 transformation, *Dalton Trans.*, 2021, **50**, 3848-3853.

12 G. Zhang, G. Wei, Z. Liu, S. R. J. Oliver, H. Fei, A robust sulfonate-based metal-organic framework with permanent porosity for efficient CO_2 capture and conversion, *Chem. Mater.*, 2016, **28**, 6276-6281.

13 Y.-G. Lee, H. R. Moon, Y. E. Cheon, M. P. Suh, A comparison of the H_2 sorption capacities of isostructural metal-organic frameworks with and without accessible metal sites: [{Zn_2(abtc)(dmf)$_2$}$_3$] and [{Cu_2(abtc)(dmf)$_2$}$_3$] versus [{Cu_2(abtc)}$_3$], *Angew. Chem. Int. Ed.*, 2008, **47**, 7741-7745.

14 D. Ma, B. Li, K. Liu, X. Zhang, W. Zou, Y. Yang, G. Li, Z. Shi, S. Feng, Bifunctional MOF heterogeneous catalysts based on the synergy of dual functional sites for efficient conversion of CO_2 under mild and co-catalyst free conditions, *J. Mater. Chem. A*, 2015, **3**, 23136–23142.

15 Z. Gao, X. Zhang, P. Xu, J. Sun, Dual hydrogen-bond donor group-containing Zn-MOF for the highly effective coupling of CO_2 and epoxides under mild and solvent-free conditions, *Inorg. Chem. Front.*, 2020, **7**, 1995-2005.

16 Z. Xue, J. Jiang, M.-G. Ma, M.-F. Li, T. Mu, Gadolinium-based metal–organic framework as an efficient and heterogeneous catalyst to activate epoxides for cycloaddition of CO_2 and alcoholysis, *ACS Sustainable Chem. Eng.*, 2017, **5**, 2623-2631.

17 J. Song, Z. Zhang, S. Hu, T. Wu, T. Jiang, B. Han, MOF-5/*n*-Bu_4NBr: an efficient catalyst system for the synthesis of cyclic carbonates from epoxides and CO_2 under mild conditions, *Green Chem.,* 2009, **11**, 1031–1036.

18 L. Tang, S. Zhang, Q. Wu, X. Wang, H. Wu, Z. Jiang, Heterobimetallic metal–organic framework nanocages as highly efficient catalysts for CO_2 conversion under mild conditions, *J. Mater. Chem. A*, 2018, **6**, 2964–2973.

19 Z. Fan, J. Wang, W. Wang, S. Burger, Z. Wang, Y. Wang, C. Wöll, M. Cokoja, R. A. Fischer, Defect engineering of copper paddlewheel-based metal-organic frameworks of type NOTT-100: implementing truncated linkers and its effect on catalytic properties, *ACS Appl. Mater. Interfaces*, 2020, **12**, 37993-38002.

20 H. Kim, H. Moon, M. Sohail, Y. Yoon, S. F. A. Shah, K. Yim, J. Moon, Y. C. Park, Synthesis of cyclic carbonate by CO_2 fixation to epoxides using interpenetrated MOF-5/*n*-Bu_4NBr, *J Mater Sci*, 2019, **54**, 11796-11803.

21 C. Bao, Y. Jiang, L. Zhao, D. Li, P. Xu, J. Sun, Aminoethylimidazole ionic liquid-grafted MIL-101-NH_2 heterogeneous catalyst for the conversion of CO_2 and epoxide without solvent and cocatalyst, *New J. Chem.,* 2021, **45**, 13893-13901.

22 J. Gu, X. Sun, X. Liu, Y. Yuan, H. Shan, Y. Liu, Highly efficient synergistic CO_2 conversion with epoxide using copper polyhedron-based MOFs with Lewis acid and base sites, *Inorg. Chem. Front.*, 2020, **7**, 4517-4526.

23 L. Song, C. Chen, X. Chen, N. Zhang, Isomorphic MOFs functionalized by free-standing acylamide and organic groups serving as self-supported catalysts for the CO_2 cycloaddition reaction, *New J. Chem.*, 2016, **40**, 2904-2909.

24 V. Guillerm, Ł. J. Weseliński, Y. Belmabkhout, A. J. Cairns, V. D'Elia, Ł. Wojtas, K. Adil, M. Eddaoudi, Discovery and introduction of a (3,18)-connected net as an ideal blueprint for the design of metal–organic frameworks, *Nat. Chem.*, 2014, **6**, 673–680.

25 Y. Ren, Y. Shi, J. Chen, S. Yang, C. Qi, H. Jiang, Ni(salphen)-based metal–organic framework for the synthesis of cyclic carbonates by cycloaddition of CO_2 to epoxides, *RSC Adv.*, 2013, **3**, 2167–2170.